

# Thermally Stable and Shape-Adaptive Triboelectric Nanogenerators Based on Liquid Electrolytes with Low Vapor Pressure

Teklebrahan Gebrekrstos Weldemhret, Nebiyou Tadesse Debele, Sofonias Nursefa Kedir, Alemtsehay Tesfay Reda, Dohyun Kim, Kwun-Bum Chung,\* and Yong Tae Park\*

Aqueous solution-based liquid electrode triboelectric nanogenerators (TEENGs) have attracted considerable interest in recent years due to their exceptional stretchability, deformability, and inherent shape-adaptability. However, previous aqueous solution-based TEENGs face challenges related to drying, which may lead to operational failures. In this study, a low-vapor pressure liquid (LVPL) electrode TEENG (LVPL-TEENG) is presented that uses branched polyethyleneimine (bPEI) or deep eutectic solvent, choline chloride/glycerol (ChCl:Gly), to increase the stability of the TEENGs at high temperatures. The LVPL-TEENGs achieve a power density of  $\approx 6.2$  and  $4.0 \text{ W m}^{-2}$  when using bPEI and ChCl:Gly as electrodes, respectively. Furthermore, these devices have remarkable energy harvesting capabilities while being stretched up to 400%. Importantly, the LVPL-TEENGs maintain a constant electrical output after being stored at  $100^\circ\text{C}$  for 24 h. Utilizing a simple single-electrode design, the LVPL-TEENGs can efficiently harvest various small physiological movements, i.e., finger bending, grasping a coffee cup, or clicking a computer mouse. Additionally, the LVPL-TEENGs have the potential to function as self-powered tactile sensors to detect the touch of any material object, indicating promising applications in the realm of human-machine interaction. This study opens new avenues for deploying stretchable and shape-adaptable TEENGs operating at high temperatures.

## 1. Introduction

The integration of small, intelligent wearable devices into the human body presents an opportunity to access vital information regarding an individual's health, lifestyle choices, and professional engagements. Because these devices rely on batteries to operate, the problems of frequent recharging and replacement, combined with their sometimes heavy nature, have become a major issue that needs attention.<sup>[1]</sup> Thus, there is a strong impetus to innovate a wearable device that can function independently without external power sources. Among the range of potential candidates, triboelectric nanogenerators (TEENGs) have been identified as promising energy conversion devices due to their simple design, lightweight structure, and affordability. Additionally, a TEENG can efficiently collect mechanical energy from human motion that would normally be wasted. In this respect, the TEENG offers a remarkably appropriate solution for the energy needs of wearable electronics. Since Professor Wang and his team launched the TEENGs in 2012,<sup>[2]</sup> researchers have carried out many

studies to create different forms of these devices, leading to several innovative designs and applications.<sup>[3–20]</sup> However, traditional TEENGs mostly utilize rigid materials such as metals or plastic plates, limiting their potential applications.<sup>[21]</sup> This limitation is particularly relevant in the context of biomechanical and physiological sensing, where the ideal TEENG should have softness, comfort, and considerable elasticity. To meet these requirements, TEENGs with favorable softness and stretchability have recently been developed using hydrogels, organohydrogels, and ionogels.<sup>[22]</sup> However, these innovative TEENGs face two main difficulties. The first problem is the tensile mismatch between the gel and its encapsulating layer (e.g., silicone rubber), which has a negative impact on the output power and the usability of the device in applications requiring flexibility and deformability.<sup>[22]</sup> The second problem is that these TEENGs have confined stretchability and deformability, which make them unsuitable for the requirements of shape-adaptable electronic systems.<sup>[21,23]</sup>

T. G. Weldemhret, K.-B. Chung  
Department of Physics  
Dongguk University  
Seoul 04620, Republic of Korea  
E-mail: kbchung@dongguk.edu

N. T. Debele, S. N. Kedir, A. T. Reda, D. Kim, Y. T. Park  
Department of Mechanical Engineering  
Myongji University  
116 Myongji-ro, Cheoin-gu, Yongin, Gyeonggi-do 17058, Republic of Korea  
E-mail: ytpark@mju.ac.kr

The ORCID identification number(s) for the author(s) of this article can be found under <https://doi.org/10.1002/smll.202500318>

© 2025 The Author(s). Small published by Wiley-VCH GmbH. This is an open access article under the terms of the [Creative Commons Attribution-NonCommercial-NoDerivs](#) License, which permits use and distribution in any medium, provided the original work is properly cited, the use is non-commercial and no modifications or adaptations are made.

DOI: 10.1002/smll.202500318

In comparison, a flexible single-electrode TENG using a liquid electrode (LS-TENG) is a highly promising option for wearable applications.<sup>[24–28]</sup> The LS-TENG has a flexible outer shell that encases a liquid interior. The outer shell acts as a triboelectric layer and the liquid component acts as an electrode responsible for collecting the electrical charge. This novel design presents many advantages. First, LS-TENG exhibits remarkable adaptability to various essential characteristics, such as shape, stretchability, flexibility, softness, and transparency, because the liquid takes on the properties of the containing/encapsulating material.<sup>[21,29]</sup> Second, LS-TENG unique combination of tribo-electronegative and tribo-electropositive friction layers in one structure, which offers several important advantages. One key benefit is that LS-TENG is not limited to triboelectric materials for the top layer, enabling energy harvesting from a wide range of objects. Moreover, the absence of a physical air gap between the triboelectric layers makes it easier to integrate seamlessly into skin-mounted electronic devices, rendering them particularly beneficial for wearable technology.<sup>[30]</sup> Furthermore, this design characteristic allows for energy harvesting from various minor physiological activities, including finger, elbow, wrist, and knee movements, as well as touch interactions involving both fingers and feet.<sup>[30]</sup>

This area of research is currently of high interest, with the limited number of reported LS-TENGs being classified into three categories: liquid metals,<sup>[29,31,32]</sup> aqueous solutions,<sup>[1,23,33–36]</sup> and nanoparticle (NP) dispersions,<sup>[21,22,30]</sup> based on the characteristics of the liquid electrode used. However, many of the LS-TENGs that have been developed so far present several problems.<sup>[24,27,28,37]</sup> Liquid metals have excellent conductivity and heat resistance, but lack transparency and require complex synthesis methods. Aqueous solutions, although transparent, suffer from issues such as evaporation and reduced functionality at higher temperatures. In particular, the water in aqueous LS-TENGs tends to evaporate even when encapsulated in waterproof materials like PDMS, resulting in significant dehydration, which adversely affects performance.<sup>[38,39]</sup> Additionally, a sodium chloride-based aqueous electrode may vaporize at 100 °C, creating pressure inside the sealing material, which makes energy harvesting at high temperatures difficult (Figure S1B, Supporting Information). On the other hand, aqueous dispersions of NPs, such as graphene oxide or MXene, are hampered by their high cost, in addition to their lack of transparency and problems of evaporation. Together, these challenges have an impact on the effectiveness and practical application of each type of liquid electrode in advancing the LS-TENGs. Therefore, developing LS-TENGs that are both cost-effective and temperature-stable, while maintaining an acceptable level of transparency, remains a major challenge to meet the demands of the rapid expansion of wearables.

One approach to creating low-cost and high-temperature stable LS-TENGs with satisfactory transparency is to use liquid electrodes that demonstrate robust stability at elevated temperatures. Potential candidates meeting these criteria include branched polyethyleneimine (bPEI) and a mixture of choline chloride and glycerol (ChCl:Gly). bPEI is an amorphous organic polymer characterized by its thermal stability due to the hydrogen bonding between adjacent free and charged amine groups.<sup>[40]</sup> It also exhibits significant ionic conductivity at ambient and elevated

temperatures as a result of its highly charged primary (25%), secondary (50%), and tertiary (25%) cationic amine groups.<sup>[41]</sup> Moreover, bPEI is a cheap and widely available organic polymer with a high propensity for charge donation due to its plentiful amine groups. For example, its incorporation into solid TENGs, whether by coating cellulose paper<sup>[42]</sup> or by combining it with other polymers,<sup>[41,43,44]</sup> has been shown to significantly enhance the TENG performance. Meanwhile, ChCl:Gly is a deep eutectic solvent (DES) made from choline chloride and glycerol, resulting in larger non-symmetric ions, which yield a liquid at room temperature with a high boiling point.<sup>[45]</sup> This DES is noted for its high electrical conductivity, excellent thermal stability, and low vapor pressure.<sup>[45]</sup> Additionally, ChCl:Gly is easy to prepare, cost-effective, non-toxic, and biodegradable, making it a better choice for the development of non-dehydrating LS-TENGs. However, despite the promising properties of bPEI and ChCl:Gly as liquid electrodes for LS-TENGs, their performance has not been thoroughly investigated.

This study developed a low vapor pressure liquid TENG (LVPL-TENG) with bPEI or ChCl:Gly as a liquid electrode and Ecoflex as both a tribo-electronegative layer and packaging material. The resulting LVPL-TENGs demonstrated excellent mechanical properties, such as stretchability, flexibility, and softness, as well as semi-transparency and remarkable thermal stability at high temperatures. Notably, these devices displayed outstanding energy harvesting capabilities while being stretched, and they maintained consistent output performance even after exposure to 100 °C for 24 h, overcoming the dehydration problems associated with previously developed LS-TENGs. Using a simple single-electrode architecture, the LVPL-TENGs were used as self-powered sensors capable of detecting a variety of physiological movements, including human body motions, grabbing a coffee cup, clicking a computer mouse, and so on. Furthermore, the shape-adaptability of LVPL-TENGs made it easier to develop and test TENG-wearing bracelet configurations. Lastly, a self-powered 4 × 4 tactile sensor was fabricated for touch perception. Due to the unique LVPL-TENG structure, which combines both tribo-electronegative and tribo-electropositive layers in one structure, the array of sensors can detect applied pressure from any object.

## 2. Results and Discussion

### 2.1. Materials and Experimental Section

The preparation process of the LVPL-TENGs using the bPEI or ChCl:Gly system is illustrated in Figure 1A. The photograph of the ChCl:Gly LVPL-TENG and operating principles of the LVPL-TENGs is shown in Figure 1D. The LVPL-TENGs have a simple structure, primarily of three basic components: 1) a liquid electrode (either bPEI (Figure 1B) or ChCl:Gly (Figure 1C)) capable of moving and deforming to ensure a continuous contact with the dielectric material (Ecoflex); 2) Ecoflex, which acts as both a negative triboelectric layer and packaging material and facilitates the generation of triboelectric charges; and 3) electrodes/metal contacts that capture the generated charges and channel them through an external circuit. The mechanism of electricity generation in LVPL-TENGs unfolds through several stages. Human skin (e.g., a finger) acts as the ground, and the LVPL-TENG

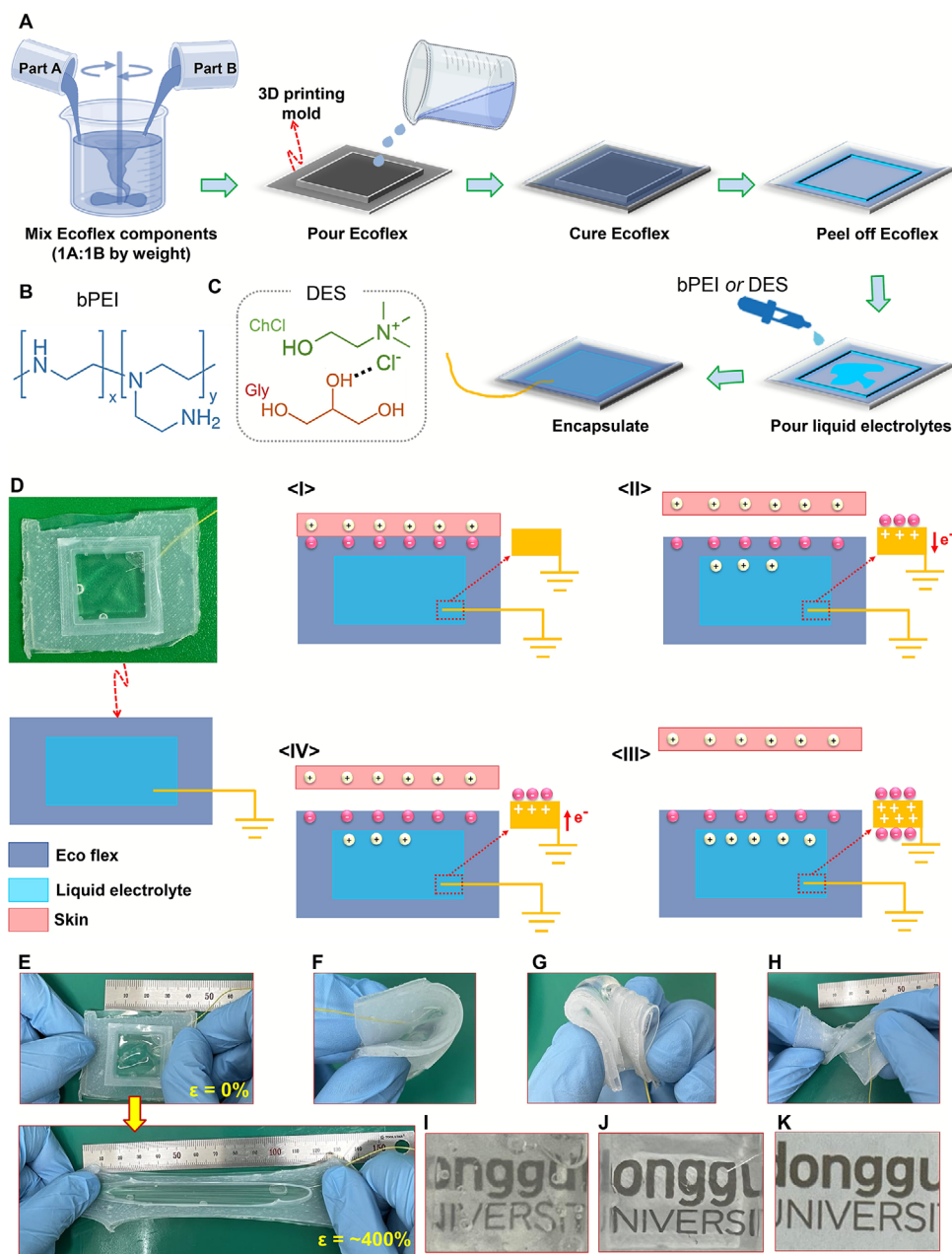


**Figure 1.** A) Schematic illustration for the fabrication process of the LVPL-TENGs. B) Chemical molecular structure of bPEI. C) Chemical molecular structure of the ChCl:Gly DES. D) Schematic illustration of the electricity-generating mechanism of the LVPL-TENGs. Photographs of the as-prepared ChCl:Gly LVPL-TENG at different deformed states, including E) stretching, F) bending, G) folding, and H) twisting. Optical images of I) bPEI-based LVPL-TENG, J) ChCl:Gly-based LVPL-TENG, and K) glass (as a reference) to demonstrate the transparency of the LVPL-TENGs.

attached to the human body acts as a single-electrode TENG (Figure 1D). When the skin contacts the LVPL-TENG, the skin and the Ecoflex come into contact, resulting in an exchange of electrons and the formation of an equal number of triboelectric charges-negative charges in the Ecoflex and positive charges in the skin (Figure 1D-I). At this point, the charges are balanced and no electrical signal is detected. As the skin moves away from the Ecoflex, it generates a positive charge on the liquid electrode, causing free electrons to flow through the external circuit from the liquid electrode to the ground, thus creating an electrical sig-

nal (Figure 1D-II). When the skin is positioned further away from the Ecoflex, the negative charges on the Ecoflex are completely balanced by the positive charges on the liquid electrode, and no electricity is produced (Figure 1D-III). When the skin returns to the Ecoflex, the positive charge induced in the liquid electrode decreases, causing electrons to flow from the ground to the liquid electrode, producing a reverse electric current (Figure 1D-IV). Through a continuous cycle of contact and separation, alternating current can be generated and used to power electronic devices.

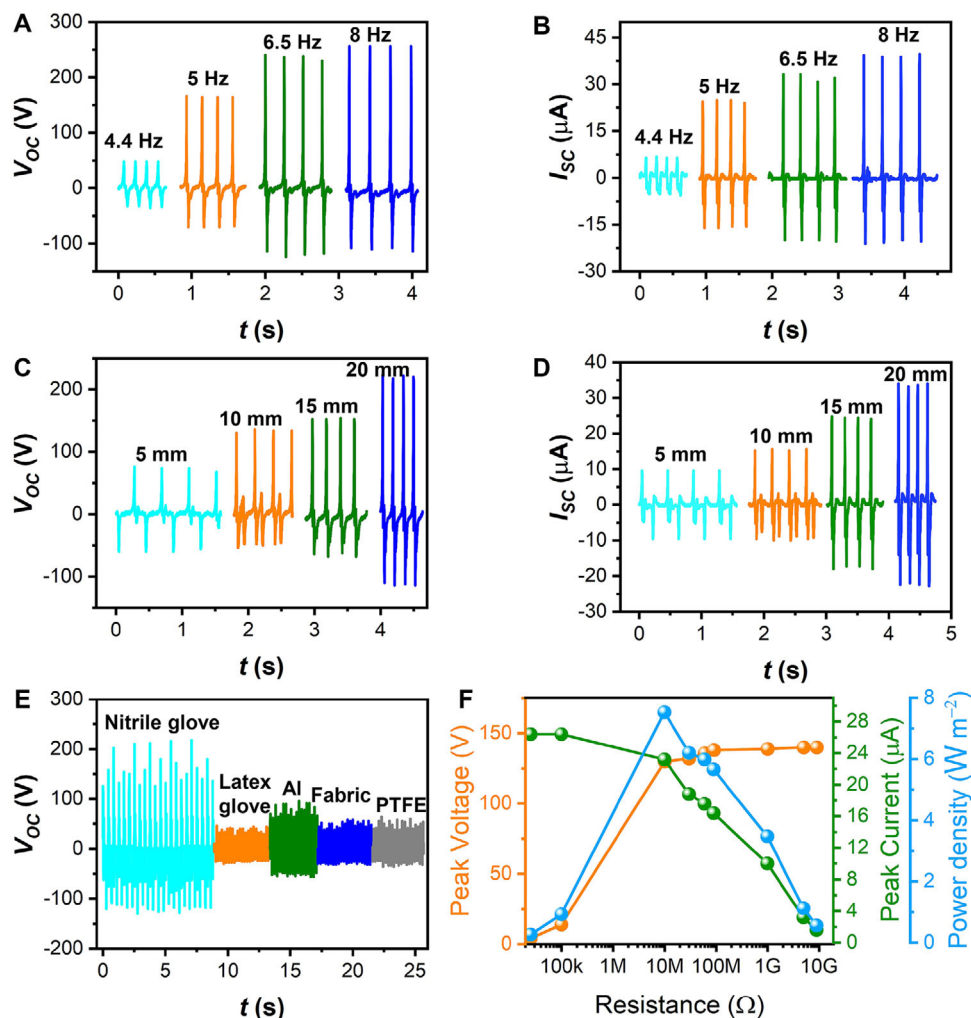


**Figure 2.** Electrical outputs of the bPEI LVPL-TENG. A–D) Electrical outputs ( $V_{OC}$ ,  $I_{SC}$ ) under different motion frequencies and gap distances. E) The output voltage of bPEI LVPL-TENG with relative contact-separation motion to different materials. F) Effect of external resistance loads on the output signals of the bPEI LVPL-TENG.

One of the fundamental advantages of liquid-based TENGs lies in their extraordinary flexibility, softness, and ability to conform to varied shapes while maintaining consistent conductivity despite undergoing different types of deformation.<sup>[29]</sup> The photograph of the LVPL-TENG under various deformation states such as stretching (Figure 1E), bending (Figure 1F), folding (Figure 1G), and twisting (Figure 1H) vividly demonstrates the device's capability to withstand extreme deformations. The remarkable mechanical characteristics of Ecoflex, particularly its high stretchability and low Young's modulus (Figure S2, Supporting Information), allow the LVPL-TENGs to be extended by as much as 400% (Figure 1E). The LVPL-TENGs' substantial elasticity and deformability make them suited for deployment on the curved surfaces of human skin, allowing for the effective harvesting of biomechanical energy generated by the movement of the human body. The photographic image of the bPEI (Figure 1I and Figure S3A, Supporting Information) and ChCl:Gly (Figure 1J; Figure S3B, Supporting Information) based LVPL-TENGs along with a glass slide (Figure 1K; Figure S3C, Supporting Informa-

tion) is provided for visual comparison of the devices' transparency. As can be seen, the LVPL-TENGs exhibit remarkable transparency.

## 2.2. Electrical Output Performance of the LVPL-TENGs

The output performance of TENGs is notably influenced by the frequency of the mechanical forces applied to them. Therefore, it is essential to investigate this relationship to optimize the design of TENGs for applications in energy harvesting and sensing. The electrical output characteristics, specifically the open-circuit voltage ( $V_{OC}$ ) and short-circuit current ( $I_{SC}$ ), of the LVPL-TENGs were analyzed within a frequency range of 4.4–8.0 Hz while maintaining a constant distance of 10 mm between the LVPL-TENG and the contact material (nitrile glove). The findings are illustrated in Figure 2A,B for the bPEI LVPL-TENG and Figure 3A,B for the ChCl:Gly LVPL-TENG. When the frequency increases from 4.4 to 8.0 Hz, the  $V_{OC}$  can rise from  $\approx 75$

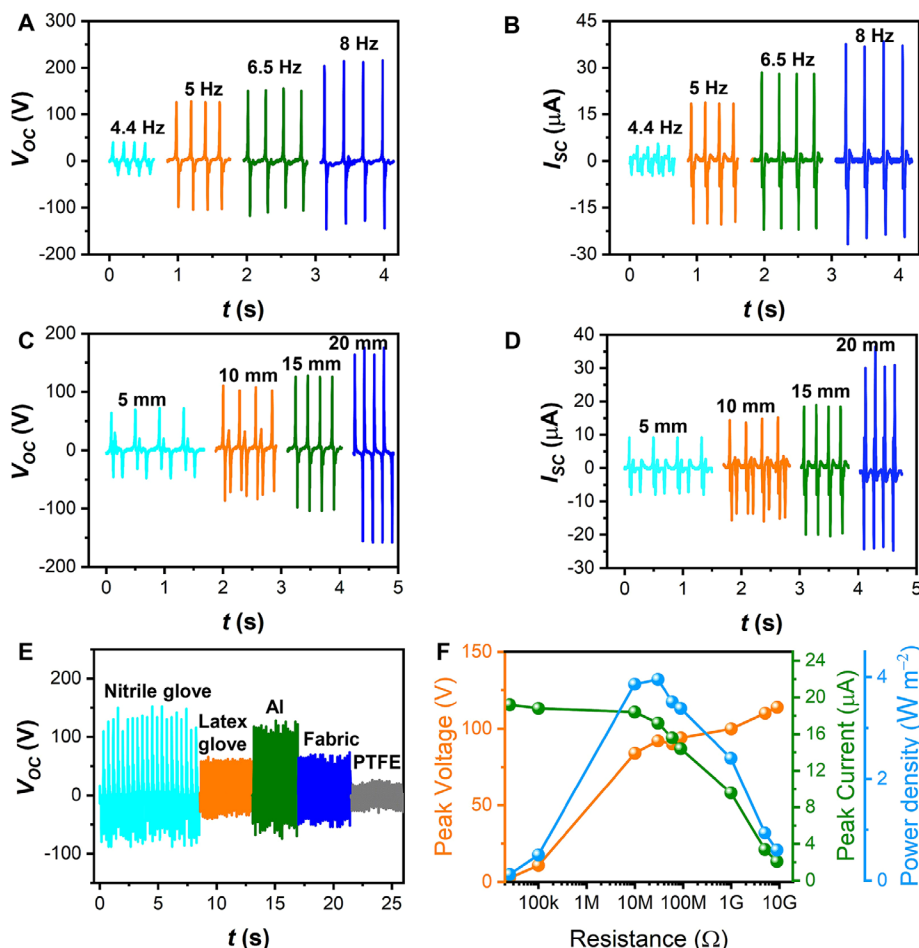


**Figure 3.** Electrical outputs of the ChCl:Gly LVPL-TENG. A–D) Electrical outputs ( $V_{OC}$ ,  $I_{SC}$ ) under different motion frequencies and gap distances. E) The output voltage of ChCl:Gly LVPL-TENG with relative contact-separation motion to different materials. F) Effect of external resistance loads on the output signals of the ChCl:Gly LVPL-TENG.

to 225 V (Figure 2A), and the  $I_{SC}$  can increase from  $\approx 10$  to 34  $\mu A$  (Figure 2B) for the bPEI LVPL-TENG. Similarly, the  $V_{OC}$  and  $I_{SC}$  of ChCl:Gly TENG increase from  $\approx 70$  to 177 V (Figure 3A) and from 9.4 to 30  $\mu A$  (Figure 3B) when the frequency rises from 4.4 to 8.0 Hz, respectively. According to the impulse-momentum change theorem (impulse ( $F\Delta t$ ) = momentum ( $m\Delta v$ ), where  $m$  is the mass of material,  $t$  is time, and  $v$  is velocity), when the LVPL-TENGs and the contacting material (nitrile glove) collide, increasing the frequency increases the speed and acceleration of the impact force, resulting in an increase in contact area, which consequently increases the surface triboelectric charge density.<sup>[41]</sup> At higher frequencies, the contact-separation speed between the LVPL-TENGs and the nitrile is faster, resulting in quicker charging-discharging and a higher electron flow rate.

The distance between the LVPL-TENGs and the nitrile has a significant impact on the TENGs' electrical output. Consequently, the effect of varying this gap distance on the performance output of the LVPL-TENGs was investigated, maintaining a constant impact frequency of 5 Hz. As the gap distance between the LVPL-TENGs and the nitrile was increased from 5 mm to 20 mm, there was a notable enhancement in both the  $V_{OC}$  and  $I_{SC}$

values for both bPEI (Figure 2C,D) and ChCl:Gly (Figure 3C,D) LVPL-TENGs. These findings are aligned with those reported in earlier research,<sup>[46]</sup> where the increase in gap distance up to 20 mm resulted in a rise in both  $V_{OC}$  and  $I_{SC}$ . This phenomenon is attributed to a more substantial accumulation of triboelectric charges, which subsequently enhances the strength of the electric field.

The electrical performance of the LVPL-TENGs with different contacting materials, including nitrile, latex, aluminum foil (Al), textile fabric, and PTFE film, was examined. In both the bPEI and ChCl:Gly LVPL-TENGs, nitrile produced the highest electrical output, followed by aluminum, whereas the electrification associated with latex, fabric, and PTFE was comparatively lower (see Figures 2E and 3E). The effectiveness of aluminum was notably greater in the ChCl:Gly LVPL-TENG, achieving a  $V_{OC}$  value nearly equivalent to that of nitrile. The results show that, in addition to the triboelectric polarity of the encapsulating Ecoflex, the polarity of the liquid electrolyte has a considerable influence on the interaction between the liquid TENG and contacting materials. Furthermore, the bPEI and ChCl:Gly LVPL-TENGs are capable of generating output voltages exceeding 800 and 600 V, respectively, when they are forcefully tapped by human skin (hand

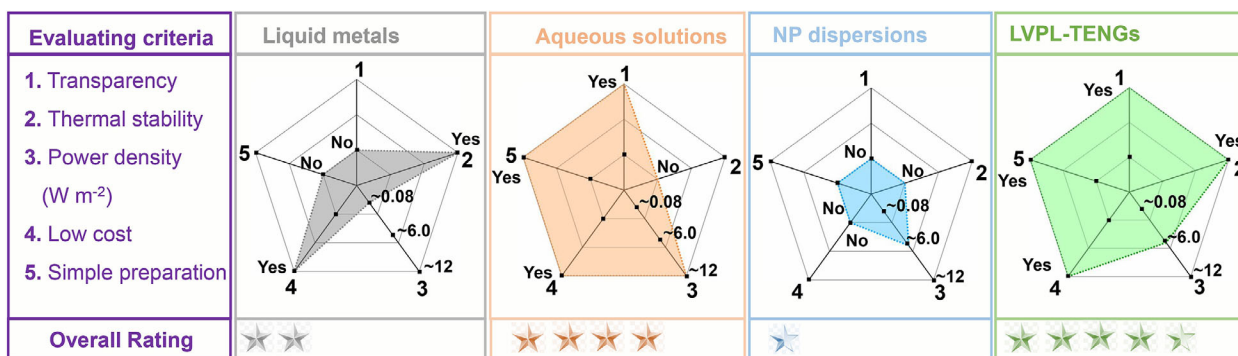


**Figure 4.** Comparison of various TENGs that utilize liquid electrodes for flexible and wearable applications: liquid metals,<sup>[29,31,32]</sup> aqueous solutions,<sup>[1,23,33–35]</sup> NP dispersions,<sup>[21,22]</sup> and LVPL-TENGs.

palm) under single-electrode configuration (Figure S4, Supporting Information).

Analyzing the relationship between external load resistance and the output power of TENGs is critical for improving their design and functionality in energy harvesting applications. Consequently, the dependence of  $V_{OC}$ ,  $I_{SC}$ , and power density on external resistance for LVPL-TENGs was investigated. As the external load resistance increased, the  $V_{OC}$  exhibited a rising trend, whereas the  $I_{SC}$  demonstrated a declining trend (refer to Figures 2F and 3F). The peak power densities recorded were  $6.20 \text{ W m}^{-2}$  for the bPEI LVPL-TENG and  $3.95 \text{ W m}^{-2}$  for the ChCl:Gly LVPL-TENG, both occurring at a matching load resistance of  $3 \text{ M}\Omega$ . These findings indicate that the bPEI LVPL-TENG outperforms the ChCl:Gly LVPL-TENG in terms of power density.

A performance comparison of the LVPL-TENGs against previously reported LS-TENGs, considering factors like power density, thermal stability, transparency, cost, and ease of preparation, is depicted in the radar chart Figure 4. While the LVPL-TENGs exhibited a relatively modest power density compared to certain aqueous solution-based TENGs,<sup>[33]</sup> they outperform the previous LS-TENGs in all these other aspects. Our LVPL-TENGs also have several distinct advantages when compared to other types of stretchable and high-temperature operable TENGs, such as organohydrogels,<sup>[47–50]</sup> ionogels,<sup>[51–56]</sup> and eutecticgels.<sup>[57–59]</sup> Notably, the power density of the LVPL-TENGs outperforms the previously reported high-temperature stable TENGs, as evidenced in Table S1 (Supporting Information). Furthermore, it effectively addresses the issues associated with tensile mismatch, limited stretchability, and deformability, as well as design constraints that are commonly encountered with organohydrogels, ionogels, and eutecticgels, as seen in Figure S5 (Supporting Information). These outstanding properties strongly support the potential of our LVPL-TENGs as thermostable and shape-adaptable nanogenerators.

### 2.3. Robustness and High-Temperature Tolerance of the LVPL-TENGs

The remarkable flexibility and stretchability of the LVPL-TENGs allow them to retain their operational capabilities even when subjected to substantial deformations. An investigation was con-

ducted on the performance of the LVPL-TENGs ( $2 \times 2 \text{ cm}^2$ ) across various states of stretching. The results indicate that the peak-to-peak voltage ( $V_{pp}$ ) slightly increases ( $\approx 19\%$  enhancement for bPEI and  $9\%$  for ChCl:Gly) when stretched to  $100\%$ , followed by a slight decline thereafter (Figure 5A,B). The observed phenomenon can be attributed to variations in the contact surface area. When the device is stretched, the contact surface area initially increases and then decreases when the device is stretched significantly (Figure 5C). Consequently, this change in surface area leads to corresponding changes in output performance. Similar trends were observed for previously reported liquid TENGs, including those using liquid metals<sup>[29,32]</sup> and MXene dispersions.<sup>[30]</sup>

One of the major issues with previously reported liquid-based TENGs is the dehydration of the aqueous solvent, which limits their use in high-temperature settings. The thermal stability of the LVPL-TENGs was assessed by incubating them in an oven at  $100 \text{ }^\circ\text{C}$  for 24 h, after which the voltage and current outputs were immediately measured. Figure 5D–I illustrates the high-temperature stability of the LVPL-TENGs. A comparative analysis was also performed on the stability of the aqueous-based liquid TENG using a NaCl solution (10 wt.%). Initially, the  $V_{pp}$  and peak-to-peak current ( $I_{pp}$ ) of the NaCl liquid TENG were  $\approx 193 \text{ V}$  and  $31 \text{ }\mu\text{A}$ , respectively. However, after being stored for 24 h in an oven at  $100 \text{ }^\circ\text{C}$ , the  $V_{pp}$  and  $I_{pp}$  significantly decreased to  $\approx 11 \text{ V}$  and  $3 \text{ }\mu\text{A}$ , retaining only  $\approx 6\%$  of the original  $V_{pp}$  and  $10\%$  of the  $I_{pp}$ . In contrast, the  $V_{pp}$  and  $I_{pp}$  of the LVPL-TENGs remained stable after being subjected to 24 h in an oven at  $100 \text{ }^\circ\text{C}$ , attributed to the superior thermal stability of bPEI and ChCl:Gly. For instance, the  $V_{pp}$  and  $I_{pp}$  of bPEI LVPL-TENG before and after being stored in an oven at  $100 \text{ }^\circ\text{C}$  were  $212 \text{ V}$  and  $40 \text{ }\mu\text{A}$  and  $217 \text{ V}$  and  $39 \text{ }\mu\text{A}$ , respectively. Additionally, the NaCl solution TENG undergoes vaporization at  $100 \text{ }^\circ\text{C}$ , resulting in pressure generation that causes the Ecoflex bag to expand (Figure S1B, Supporting Information). This phenomenon can lead to exploding and complicating the process of tapping the TENG and harvesting energy at elevated temperatures. In contrast, our LVPL-TENG does not induce expansion of the Ecoflex bag and preserves its original structure even at high temperatures (Figure S1A, Supporting Information).

To further illustrate the thermal stability of the LVPL-TENGs, thermogravimetric analysis (TGA) of bPEI and ChCl:Gly was conducted in a nitrogen atmosphere, and the results were

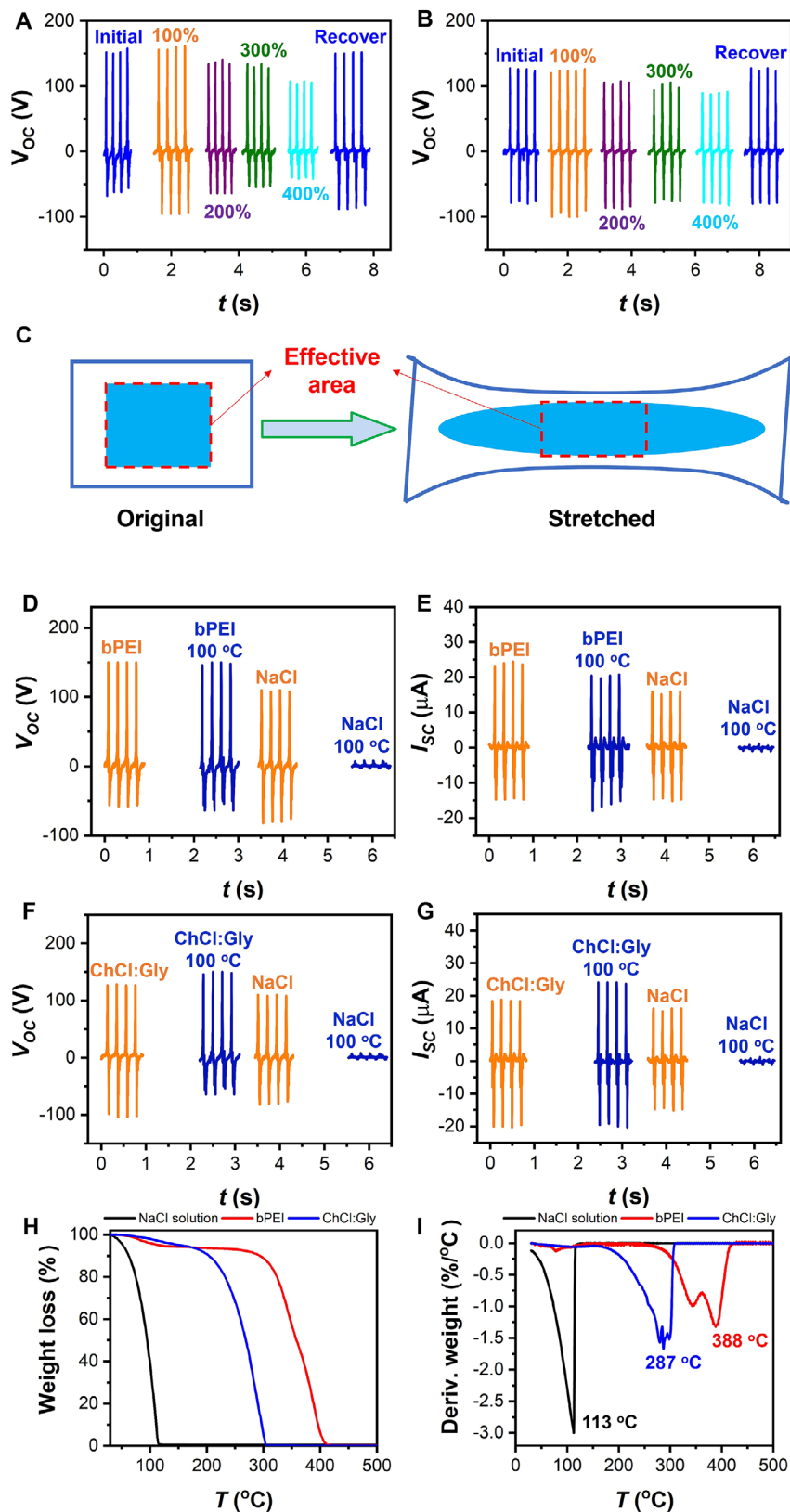


**Figure 5.** Examination of electrical outputs under various stretching states for the A) bPEI and B) ChCl:Gly LVPL-TENGs. C) Schematic illustration of the effective area changes during stretching. D–G) Comparison of the electrical outputs of the LVPL-TENGs (D,E for bPEI and F,G for ChCl:Gly) and NaCl-based liquid TENG before and after being stored at 100 °C for 24 h. TGA H) and I) DTG curves for bPEI, ChCl:Gly, and NaCl solution.

compared with that of NaCl. The TGA and derivative thermogravimetry (DTG) curves are presented in Figure 5H,I, with the corresponding thermal parameters provided in Table S2 (Supporting Information). The maximum decomposition temperatures ( $T_{max}$ ) for bPEI and ChCl:Gly were recorded at 388 and 287 °C, respectively, significantly exceeding the  $T_{max}$  of the NaCl solution, which was only 113 °C. Additionally, the temperatures corresponding to a 5 wt.% mass loss ( $T_{5\%}$ ) were found to be 53, 118, and 154 °C for NaCl, bPEI, and ChCl:Gly, respectively (Table S2, Supporting Information), thereby reinforcing the high-temperature tolerance of the LVPL-TENGs. Moreover, the LVPLs demonstrated a lower DTG peak value in comparison to NaCl, indicating a reduced rate of thermal decomposition (Figure 5I; Table S2, Supporting Information).

Temperature-dependent performance analysis was also carried out to further assess the thermal stability of the LVPL-TENGs. In this test, the devices were incubated on a hot plate at various temperatures for 5 min, after which the voltage output was recorded by manually tapping the TENGs. The output performance of the LVPL-TENGs demonstrated remarkable stability across a temperature range from R.T. to 100 °C (Figure S6 and Movie S3, Supporting Information), demonstrating their substantial potential for use in high-temperature situations.

The application and longevity of a TENG are significantly influenced by its robustness, durability, and reproducibility. Therefore, the cyclic output stability of the LVPL-TENGs was assessed through extended motion cycles, as illustrated in Figure S7A,B (Supporting Information). The results indicate that the LVPL-TENGs consistently exhibit a stable electrical output even after 50000 cycles of repetitive contact-separation motion. This finding suggests that the LVPL-TENGs possess durability comparable to that of other solid-based TENGs. It is important to note that the cyclic durability test was concluded at 50000 iterations due to time constraints, and this figure does not represent the maximum cycle limit. In addition, the cyclic stability of the LVPL-TENGs at elevated temperature (100 °C) was tested, and no degradation of output voltage was observed for 1000 cycles (Figure S7C,D, Supporting Information).

## 2.4. Applications of the LVPL-TENGs

The LVPL-TENGs have exceptional properties, including stretchability, deformability, and durability, all of which are essential for the devices' wearability. Consequently, they can be mounted to different objects (Figure S8, Supporting Information) and are capable of functioning as self-powered electronic skin (e-skin) sensors that enable monitoring of a variety of human activities. Subtle movements, such as hand tapping, grasping a coffee cup, clicking a computer mouse, typing on a keyboard, bending, stretching, and finger movements, were examined using the ChCl:Gly LVPL-TENG. The electricity generation principle for the movements involving stretching and bending is depicted in Figure 6A. When the LVPL-TENG is fully stretched or bent, the electrostatic induction and contact-electrification result in equal amounts of opposite polarity charges on the liquid ChCl:Gly and Ecoflex surfaces. At this point, there is no electron flow in the external circuit. When the pressure is released, the Ecoflex layer begins to bounce back to its original configuration, resulting in

imbalanced surface charges on both materials, allowing electrons to flow through the external circuit. Once the Ecoflex has fully restored to its initial state, the triboelectric charges become balanced, preventing any electron flow. When stretching or bending is applied again, new unbalanced frictional surface charges are created, causing the flow of electrons in the opposite direction. This sequence represents one complete cycle in the electricity generation process. By repeatedly stretching or bending the LVPL-TENG, a continuous generation of alternating electricity can be achieved. On the other hand, the mechanism for the other applications is due to a contact separation between the LVPL-TENG and human skin under single-electrode mode as illustrated in Figure 1D. As evidenced in Figure 6B–G, the device can generate an output  $V_{OC}$  of  $\approx 600, 95, 102, 97, 16,$  and  $28$  V from actions like vigorous hand tapping, grasping a coffee cup, clicking a mouse, typing on a keyboard, bending, and stretching the LVPL-TENG, respectively. Additionally, output voltages of  $\approx 2$  and  $5$  V were observed when the index finger was bent at smaller ( $60^\circ$ ) and larger ( $90^\circ$ ) angles, respectively (Figure 6H). This behavior can be ascribed to the increased contact area between the Ecoflex layer and the LVPLs when subjected to a greater bending angle. The LVPL-TENG can be affixed to the joints of the four fingers—index, middle, ring, and little—to assess the differing pressure applied as a function of the number of fingers that are bent, achieved through the detection of unique output voltage signals (Figure 6I,J). The energy produced from these movements was sufficient to energize light emitting diodes (LEDs) (Figure 6K–M; Movie S1, Supporting Information). These findings illustrate the ability of the LVPL-TENGs to monitor subtle physiological activities.

The electricity produced by the LVPL-TENGs is in the form of alternating current (AC), which is not suitable for direct use as a power source. Therefore, it is necessary to convert this AC into direct current (DC). A widely utilized method for achieving this conversion involves the implementation of a bridge rectifier that is connected to the LVPL-TENGs, facilitating the transformation of AC into DC. The resulting rectified DC can then be utilized for charging or storing energy in capacitors or batteries.<sup>[60]</sup> Figure 7A illustrates the schematic of the full bridge rectifier employed for this conversion process. As shown in Figure 7B,C, the negative outputs of both voltage and current were effectively transformed into a positive signal, maintaining the integrity of the LVPL-TENGs output. To assess the charging capabilities of the LVPL-TENGs, experiments were conducted using commercial capacitors with varying capacitances of 3.3, 33, 100, and 220  $\mu$ F. The results, depicted in Figure 7D, confirm that the LVPL-TENGs successfully charged the capacitors through the bridge rectifier.

One significant benefit of liquid-based TENGs lies in their versatility in design, allowing for the creation of TENGs in various shapes tailored to specific needs. For instance, tube-like LVPL-TENGs can be constructed using a hollow tube of Ecoflex that is filled with a ChCl:Gly DES, as illustrated in Figure 7E. When this tube-like LVPL-TENG is worn on the wrist to harvest mechanical energy, it can produce a substantial voltage that can illuminate multiple LEDs. Furthermore, the amount of electricity generated and the brightness of the LEDs increase in direct correlation with the number of fingers tapping the tube-like TENG (Figure 7F; Movie S2, Supporting Information).

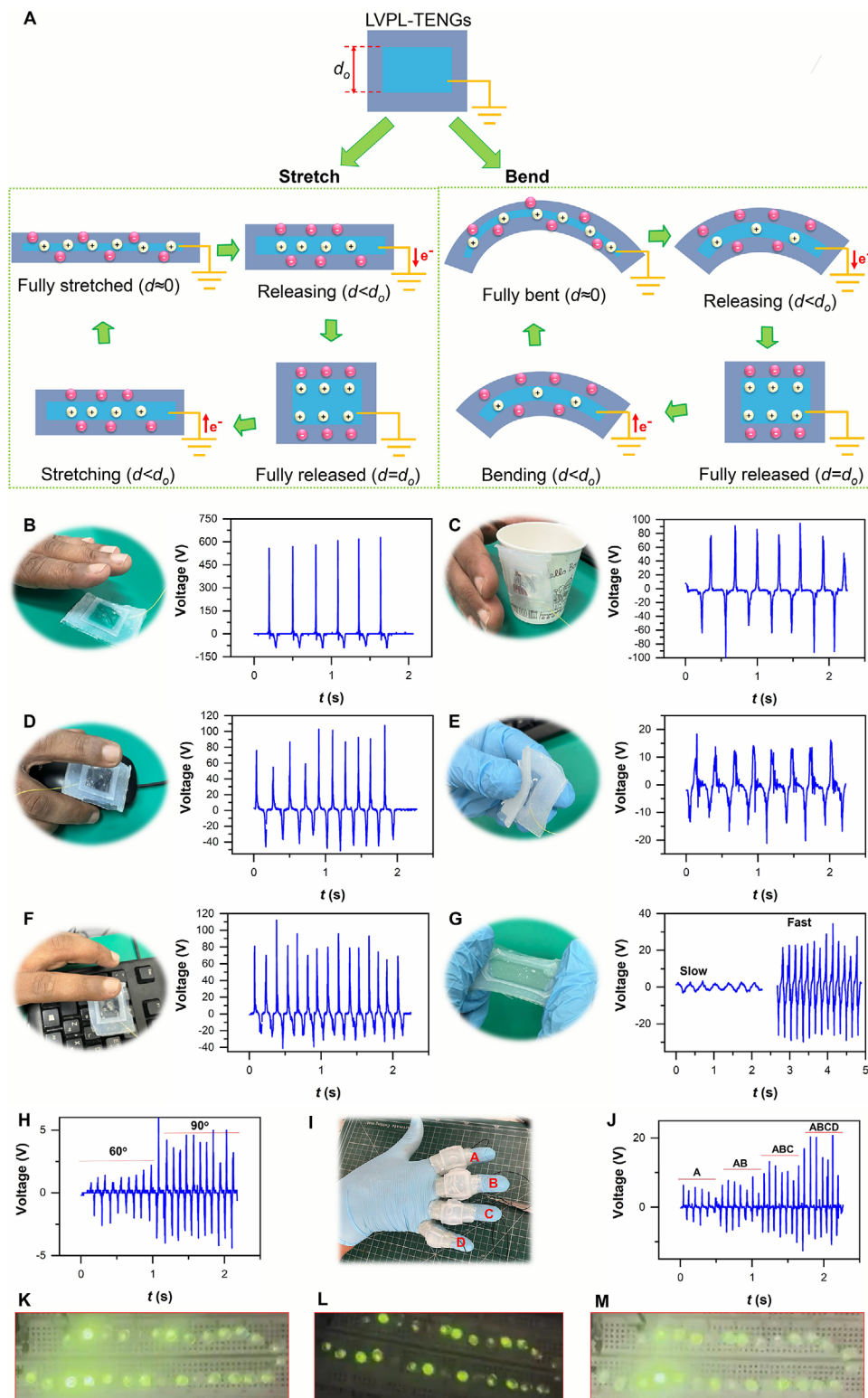


**Figure 6.** Energy harvesting from 7 types of motion using the ChCl:Gly LVPL-TENG. A) Schematic diagrams illustrating the working mechanism of the LVPL-TENG under stretching and bending.  $V_{OC}$  with B) hand tapping, C) coffee cup grabbing, D) computer mouse clicking, E) bending the TENG, F) computer keyboard typing, G) stretching the TENG, and H–J) different finger bindings. LEDs lit during K) hand tapping, L) keyboard typing, and M) coffee cup grabbing.

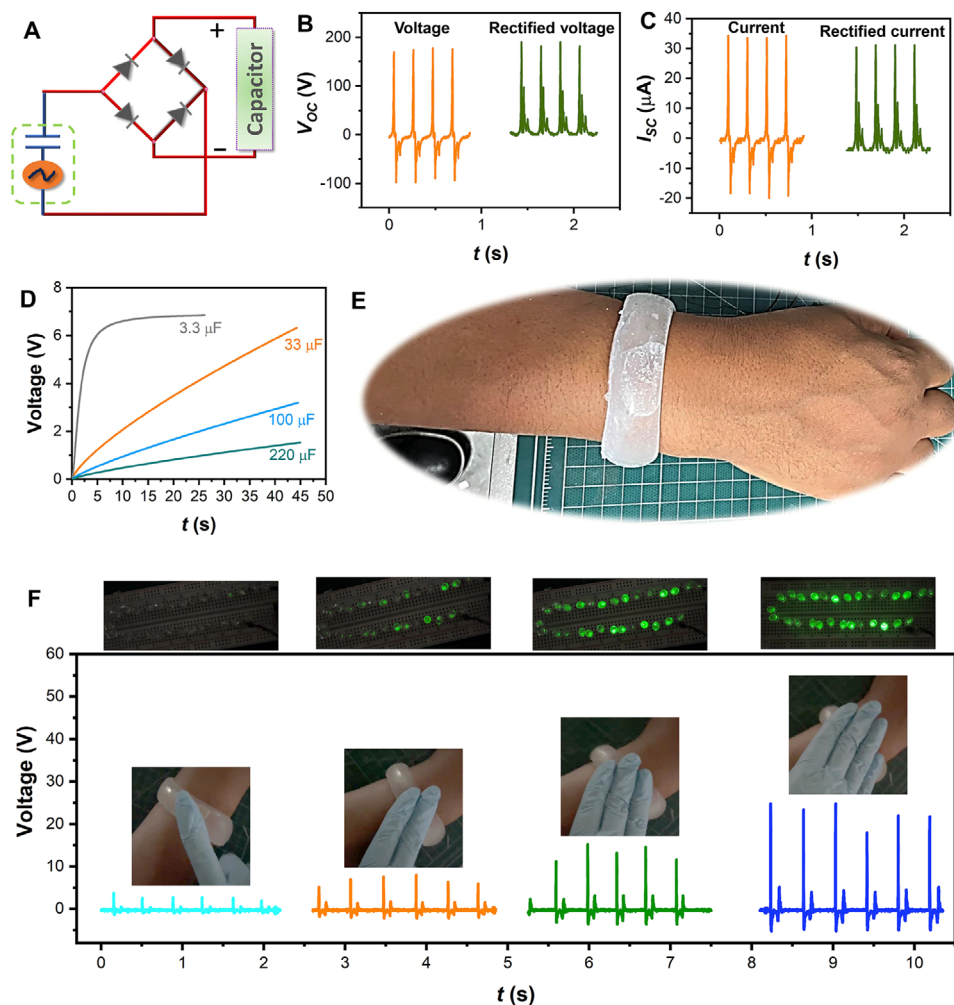


**Figure 7.** A) TENG connected to a full-wave bridge rectifier. Rectified B) voltage and C) current. D) Charging of capacitors of 3.3, 33, 100, and 220  $\mu\text{F}$ . E) Photograph of the tube-like bPEI LVPL-TENG worn on a volunteer's wrist. F) Energy harvesting from tube-like ChCl:Gly LVPL-TENG, which was worn on the wrist and activated by tapping with different fingers.

To further showcase the LVPL-TENGs' designability and shape-adaptability, a more innovative and aesthetically pleasing bracelet featuring eight cube-shaped sensors ( $1 \times 1 \times 0.5 \text{ cm}^3$ ) was developed (Figure 8A). This innovative smart bracelet is built for comfortable wear on the wrist and can generate an output voltage of more than 60 V, enough to illuminate six green LEDs upon being tapped (Figure 8B–D; Movie S4, Supporting Information). The ability of LVPL-TENGs to be designed into intricate shapes while effectively harvesting energy from mechanical movements positions them as promising candidates for integration into various shape-adaptive electronic systems.

A prototype tactile sensor has been developed to demonstrate the various applications of the LVPL-TENGs. Tactile sensors play a key role in detecting and mapping pressure/force, which are key attributes of artificial e-skin.<sup>[41]</sup> The manufacturing process of the tactile sensor is shown in Figure 9A, and details are given in the “Experimental Section”. Initially, a template with a 4-by-4 arrangement of sensor units was created by 3D printing (Figure 9A(I)). Afterward, Ecoflex was poured into the template to achieve complete coverage (Figure 9A(II)). After allowing the material to air-

dry at room temperature, the soft and flexible patterned elastomer was removed from the template, resulting in cavities in the sensor units (Figure 9A(III)). Then, bPEI was injected into these cavities and wires were attached to each end of the sensor units. To complete the assembly, a thin layer of Ecoflex was laid on top of the filled elastomer, and the two materials were bonded using a silicone adhesive (Figure 9A(IV)). After thorough air drying, a sensor array ( $\approx 9 \text{ cm} \times 9 \text{ cm} \times 0.06 \text{ cm}$ ), consisting of 16 individual units each measuring  $1 \times 1 \text{ cm}^2$  and arranged in a 4-by-4 pixel matrix, was successfully fabricated (Figure 9A(V)). To assess the sensing performance of the sensor array, various objects (nitrile, NEO battery, and toy ball) were dropped onto the e-skin. The output from the tactile sensor was presented through counter-color map visualizations (Figure 9B–D). The sensor array can detect the position of different objects through voltage modulation when these objects are in contact with the sensor. This highlights the potential of the sensor array for tactile sensing applications, especially in the area of e-skin for soft robotics, enabling the perception of external environmental stimuli.

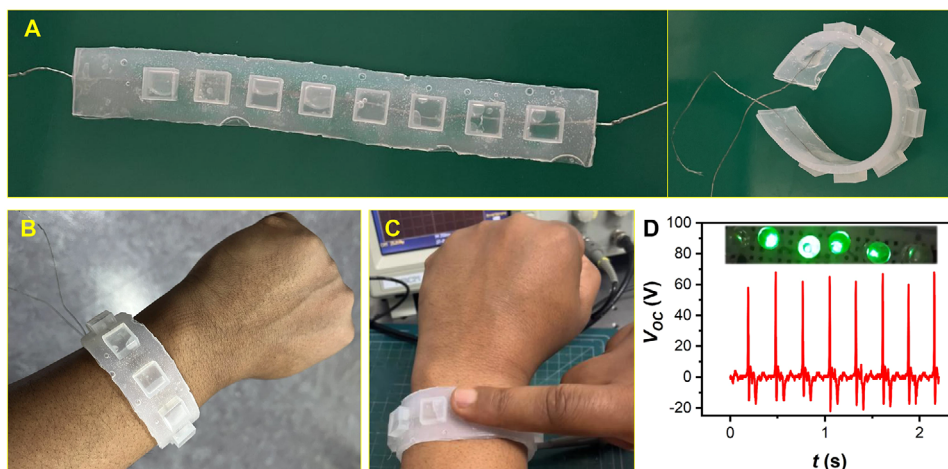


**Figure 8.** A) Optical image of the smart ChCl:Gly LVPL-TENG bracelet. B) The smart bracelet worn on a volunteer's wrist. C) Optical image of poking the smart bracelet on one of the sensors and its corresponding D) generated electrical response (inset: showcasing LEDs energized by the generated electricity).

In a complex environment populated by objects made of a variety of materials, particularly in robotic applications, it is essential that the tactile sensor is capable of efficiently detecting touch and contact under typical conditions.<sup>[61]</sup> One of the major advantages of the design framework for liquid TENGs is that they integrate both tribo-electronegative and tribo-electropositive layers into one structure. This integration differentiates our LVPL-TENG sensor array from the previously developed TENG-based tactile sensors by eliminating the material limitation of the top layer, which allows for the detection of pressure applied by any substance. The response of the tactile sensor to different forms of touch (i.e., finger tapping two sensors simultaneously) as well as its interaction with other additional materials of differing textures (AA's battery and ground tennis ball) was also assessed. The findings from these interactions are provided as a line plot in Figure S9A–D (Supporting Information). The results demonstrate that the LVPL-TENG-based tactile sensor can produce a voltage output from a variety of materials, underscoring the versatile applicability of the sensor array as a robotic e-skin. Moreover, the intensity of the output performance is influenced by the characteristics of the tapping action. For instance, applying pressure with two fingers results in an output signal (Figure S9B, Supporting Information) that is nearly double that of a single-finger tap (Figure S9A, Supporting Information), while striking the sensor forcefully with a standard tennis ball can yield a voltage as high as 255 V (Figure S9D, Supporting Information).

### 3. Conclusion

In this study, we present a triboelectric nanogenerator (TENG) with a low vapor pressure liquid (LVPL) electrode that uses either bPEI or ChCl:Gly to enhance the stability of liquid-based TENGs under high temperature conditions. The LVPL-TENG exhibits a remarkable power density:  $\approx 6.2$  and  $4.0 \text{ W m}^{-2}$  for bPEI and ChCl:Gly electrodes, respectively. Furthermore, these devices have demonstrated remarkable energy harvesting capabilities, maintaining their functionality even when stretched up to 400%. Notably, the LVPL-TENGs maintain a constant electrical output

after being subjected to temperatures of up to  $100 \text{ }^\circ\text{C}$  for 24 h. Using a simple single-electrode design, the LVPL-TENGs can efficiently capture small physiological movements such as grabbing a cup of coffee or clicking on a computer mouse. Additionally, these devices have the potential to act as self-powered tactile sensors, capable of detecting touch from variety of materials, which indicates significant applications in human-machine interaction. This study provides the basis for deploying stretchable and shape-adaptable TENGs in high temperature environments.

### 4. Experimental Section

**Materials:** Branched polyethyleimine (bPEI, average  $M_w \approx 25,000/M_n \approx 10,000$ ), choline chloride (ChCl,  $\geq 98.0\%$ ), and sodium chloride (NaCl,  $\geq 98.0\%$ ) were procured from Sigma–Aldrich. Glycerol (Gly, 99.0%) was provided by Samchun Chemicals Co., Ltd. (Korea). Ecoflex 00–30 (Smooth-On Inc., USA) and silicon adhesive (ELASTOSIL E43) were purchased from Coupang, Korea.

**Synthesis of ChCl:Gly DES:** The synthesis of ChCl:Gly was conducted following a previously established methodology.<sup>[62]</sup> Briefly, choline chloride, serving as the hydrogen bond acceptor, was combined with glycerol, the hydrogen bond donor, in a molar ratio of 1:2. Subsequently, the resulting mixture was heated at  $80 \text{ }^\circ\text{C}$  until a clear solution was achieved.

**Fabrication of the LVPL-TENGs:** The fabrication of the LVPL-TENGs, as illustrated in Figure 1A, was achieved through a straightforward process. Initially, a liquid mixture of Ecoflex 00–30 and Ecoflex 00–50 rubber was created by combining Part A and Part B in a 1:1 weight ratio within a beaker. Following thorough mixing, the Ecoflex blend was promptly poured into a pre-designed 3D printing mold to ensure complete coverage, after which it underwent a degassing process under vacuum conditions and was allowed to dry at ambient temperature. Subsequently, a flexible Ecoflex rubber structure featuring a cavity was carefully removed from the mold. The next step involved injecting liquid electrodes, either bPEI or ChCl:Gly, into the cavity of the Ecoflex rubber, and a second Ecoflex rubber template of identical dimensions was employed to encapsulate the liquid, with the two materials bonded using silicone adhesive. A copper lead wire was affixed to one side to facilitate electrical connectivity. Upon air drying, an LVPL-TENGs ( $2 \text{ cm} \times 2 \text{ cm}$ ) with a thickness of  $0.04\text{--}0.045 \text{ cm}$  was successfully produced. The tactile sensor was produced using a similar process; however, a 3D-printed mold featuring a specifically designed pattern consisting of 4-by-4 sensor units ( $1 \text{ cm} \times 1 \text{ cm}$ ) was employed.

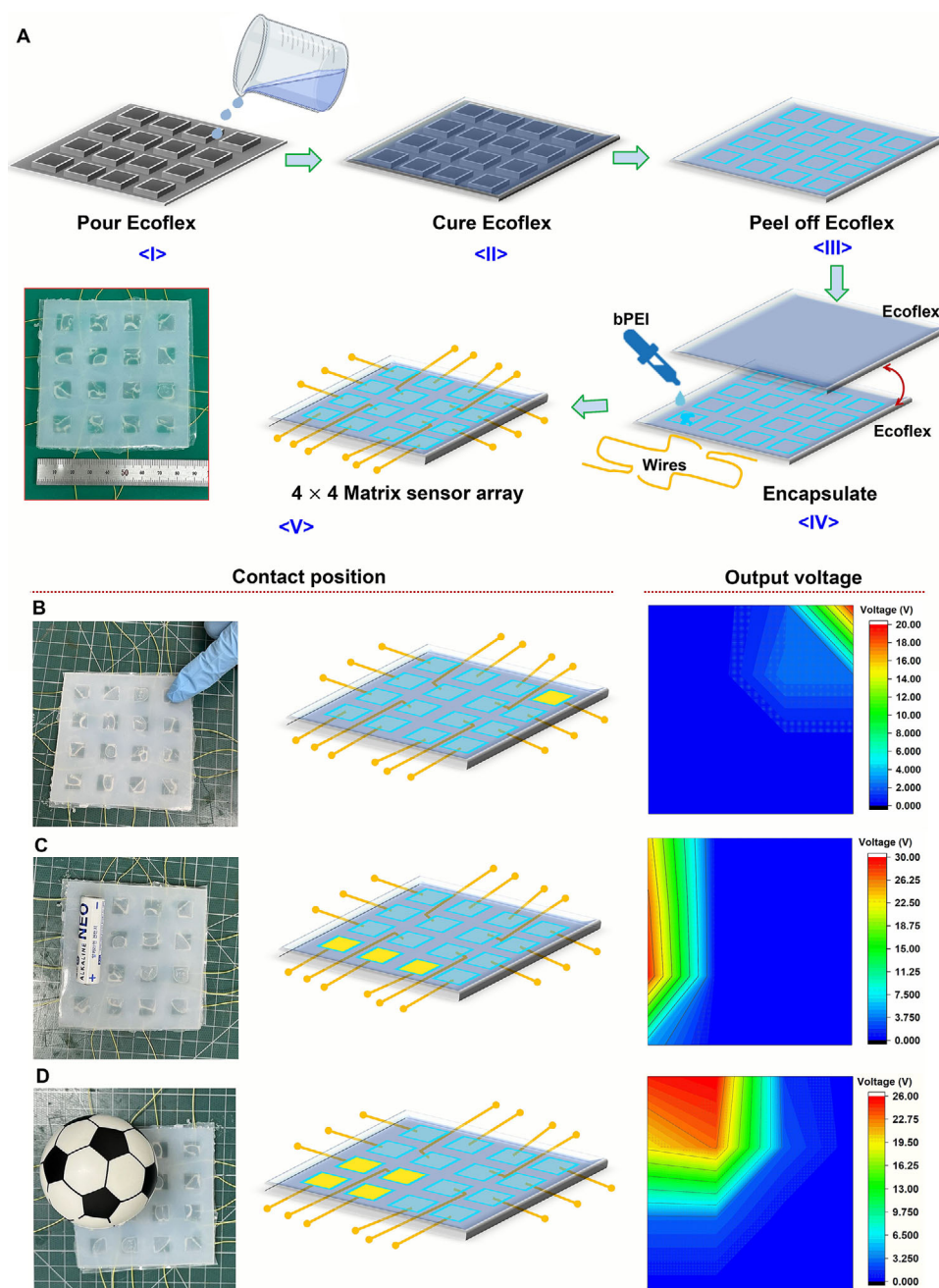


**Figure 9.** A skin-like touch sensor using the flexible and stretchable LVPL-TENG for touch perception. A) The structure of the sensor matrix and the photograph of the 4 × 4 tactile sensors. B–D) Optical images of different objects contacted the touch sensor and the corresponding mapping of the electrical response.

**Characterizing:** A thermogravimetric analyzer (Mettler Toledo, TGA2) was employed to conduct the thermogravimetric analysis of the liquid electrolytes in a nitrogen atmosphere with a flow rate of  $50 \text{ mL min}^{-1}$  and a heating rate set at  $10 \text{ }^\circ\text{C min}^{-1}$ . The triboelectric performance of the LVPL-TENGs was evaluated as depicted in Figure S10A (Supporting Information). A pushing tester (JIPT-120, Junil Tech) facilitated the contact-separation process, allowing for precise control over the contact frequency and vertical distance gap. A nitrile glove affixed to an aluminum (Al) was secured to an acrylic plate, which was subsequently mounted on a linear motor. The LVPL-TENGs were positioned on a second acrylic

plate oriented perpendicularly to the motor's movement. An oscilloscope (TDS 2012B, Tektronix) was employed to measure the open-circuit voltage ( $V_{OC}$ ). However, for recording the short-circuit current ( $I_{SC}$ ), a low-noise current preamplifier (SR570, Stanford Research Systems) was utilized along with the oscilloscope. Data acquisition from the oscilloscope was carried out using Tektronix OpenChoice version 2.8 software. For the performance assessment, one terminal of the oscilloscope was connected to the LVPL-TENGs, while the other terminal was linked to the nitrile glove/Al layer, thereby establishing the testing circuit (Figure S10A, Supporting Information). The output performance was obtained at varying

frequencies and distances between the nitrile glove and Ecoflex surfaces by fixing the contact force at 2.5 N. For applications in sensing and various biomechanical energy harvesting scenarios, a single-electrode mode was implemented (Figure S10B, Supporting Information). In this configuration, one terminal of the oscilloscope was connected to the LVPL-TENGs, while the other terminal was grounded to complete the testing circuit.

## Supporting Information

Supporting Information is available from the Wiley Online Library or from the author.

## Acknowledgements

This work was supported by the National Research Foundation of Korea (NRF) grant funded by the Korea government (MSIT) (No. 2022R1A2C2006081 and RS-2024-00352476).

## Conflict of Interest

The authors declare no conflict of interest.

## Data Availability Statement

The data that support the findings of this study are available from the corresponding author upon reasonable request.

## Keywords

energy harvesters, liquid-triboelectric nanogenerators, stretchable and deformable electronics, tactile sensors

Received: January 8, 2025

Revised: April 7, 2025

Published online: April 22, 2025

- [1] S. Y. Yun, I. W. Tcho, W. G. Kim, D. W. Kim, J. H. Son, S. W. Lee, Y. K. Choi, *J. Mater. Chem A. Mater.* **2022**, *10*, 10383.
- [2] F. R. Fan, Z. Q. Tian, Z. L. Wang, *Nano Energy* **2012**, *1*, 328.
- [3] H. G. Menge, N. D. Huynh, H. J. Hwang, S. Han, D. Choi, Y. T. Park, *ACS Energy Lett.* **2021**, *6*, 2451.
- [4] H. G. Menge, N. D. Huynh, K. Choi, C. Cho, D. Choi, Y. T. Park, *Adv. Funct. Mater.* **2023**, *33*, 2210571.
- [5] T. Gebrekrstos Weldemhret, D. W. Lee, Y. Tae Park, J. Il Song, *Chem. Eng. J.* **2022**, *450*, 137982.
- [6] T. G. Weldemhret, D. W. Lee, M. N. Prabhakar, Y. T. Park, J. I. Song, *ACS Appl. Nano Mater.* **2022**, *5*, 12464.
- [7] H. J. Hwang, J. S. Yeon, Y. Jung, H. S. Park, D. Choi, *Small* **2021**, *17*, 1903089.
- [8] K. H. Ke, C. K. Chung, *Small* **2020**, *16*, 2001209.
- [9] T. G. Weldemhret, Y. T. Park, J. I. Song, *Adv. Colloid Interface Sci.* **2024**, *326*, 103132.
- [10] M.-Z. Huang, P. Parashar, A.-R. Chen, S.-C. Shi, Y.-H. Tseng, K. C. Lim, H.-Y. Yeh, A. Pal, D.-Y. Kang, Z.-H. Lin, *Nano Energy* **2024**, *122*, 109266.
- [11] C. Yeh, F.-C. Kao, P.-H. Wei, A. Pal, K. Kaswan, Y.-T. Huang, P. Parashar, H.-Y. Yeh, T.-W. Wang, N. Tiwari, T.-T. Tsai, Y.-F. Huang, Z.-H. Lin, *Nano Energy* **2022**, *104*, 107852.
- [12] A. Pal, K. C. Lim, S.-W. Chen, Y.-T. Huang, P. Parashar, A. Ganguly, Y.-H. Chen, K.-P. Fan, L.-C. Shen, J. Cheng, Z.-H. Lin, *Device* **2024**, *2*, 100421.
- [13] T.-H. Chang, Y.-W. Peng, C.-H. Chen, T.-W. Chang, J.-M. Wu, J.-C. Hwang, J.-Y. Gan, Z.-H. Lin, *Nano Energy* **2016**, *21*, 238.
- [14] Y. T. Jao, P. K. Yang, C. M. Chiu, Y. J. Lin, S. W. Chen, D. Choi, Z. H. Lin, *Nano Energy* **2018**, *50*, 513.
- [15] J. Luo, Z. L. Wang, *EcoMat* **2020**, *2*, 12059.
- [16] W. G. Kim, D. W. Kim, I. W. Tcho, J. K. Kim, M. S. Kim, Y. K. Choi, *ACS Nano* **2021**, *15*, 258.
- [17] J. J. Shao, T. Jiang, Z. L. Wang, *Sci. China. Technol. Sci.* **2020**, *63*, 1087.
- [18] K. Luo, T. Peng, Y. Zheng, Y. Ni, P. Liu, Q. Guan, Z. You, *Adv. Mater.* **2024**, *36*, 2312500.
- [19] H. Zhang, Y. Han, Q. Guan, Z. You, M. Zhu, *Adv. Mater.* **2024**, *36*, 2403908.
- [20] Q. Guan, X. Lu, Y. Chen, H. Zhang, Y. Zheng, R. E. Neisiany, Z. You, *Adv. Mater.* **2022**, *34*, 2204543.
- [21] Y. Wu, Y. Luo, J. Qu, W. A. Daoud, T. Qi, *Nano Energy* **2019**, *64*, 103948.
- [22] X. Zhao, Z. Wang, Z. Liu, S. Yao, J. Zhang, Z. Zhang, T. Huang, L. Zheng, Z. L. Wang, L. Li, *Nano Energy* **2022**, *96*, 107067.
- [23] Y. Wu, Y. Luo, J. Qu, W. A. Daoud, T. Qi, *Nano Energy* **2020**, *75*, 105027.
- [24] A. Kulandaivel, S. Potu, A. Babu, N. Madathil, M. Velpula, R. K. Rajaboina, U. K. Khanapuram, *Nano Energy* **2024**, *120*, 109110.
- [25] Q. T. Nguyen, D. L. Vu, C. D. Le, K. K. Ahn, *Sensors* **2023**, *23*, 5888.
- [26] S. Lin, X. Chen, Z. L. Wang, *Chem. Rev.* **2022**, *122*, 5209.
- [27] A. Kulandaivel, S. Potu, R. K. Rajaboina, U. K. Khanapuram, *ACS Appl. Mater. Interfaces.* **2024**, *16*, 58029.
- [28] K. Wang, J. Li, *J. Mater. Chem. A Mater.* **2021**, *9*, 8870.
- [29] Y. Yang, N. Sun, Z. Wen, P. Cheng, H. Zheng, H. Shao, Y. Xia, C. Chen, H. Lan, X. Xie, C. Zhou, J. Zhong, X. Sun, S.-T. Lee, *ACS Nano* **2018**, *12*, 2027.
- [30] W. T. Cao, H. Ouyang, W. Xin, S. Chao, C. Ma, Z. Li, F. Chen, M. G. Ma, *Adv. Funct. Mater.* **2020**, *30*, 2004181.
- [31] L. Yang, L. Guo, Z. Wang, C. Meng, J. Wu, X. Chen, A. A. Musa, X. Jiang, H. Cheng, *Adv. Sci.* **2024**, *11*, 2405792.
- [32] Y. Yang, J. Han, J. Huang, J. Sun, Z. L. Wang, S. Seo, Q. Sun, *Adv. Funct. Mater.* **2020**, *30*, 1909652.
- [33] X. Wang, Y. Yin, F. Yi, K. Dai, S. Niu, Y. Han, Y. Zhang, Z. You, *Nano Energy* **2017**, *39*, 429.
- [34] F. Yi, X. Wang, S. Niu, S. Li, Y. Yin, K. Dai, G. Zhang, L. Lin, Z. Wen, H. Guo, J. Wang, M.-H. Yeh, Y. Zi, Q. Liao, Z. You, Y. Zhang, Z. L. Wang, *Sci Adv* **2016**, *2*, 1501624.
- [35] H. Li, *J. Electron. Mater.* **2022**, *51*, 7304.
- [36] H. Patnam, S. A. Graham, P. Manchi, M. V. Paranjape, Y. S. Huh, J. S. Yu, *Adv. Compos. Hybrid Mater.* **2024**, *7*, 54.
- [37] K. R. Kaja, S. Hajra, S. Panda, M. A. Belal, U. Pharino, H. Khanbareh, N. Vittayakorn, V. Vivekananthan, C. Bowen, H. J. Kim, *Nano Energy* **2024**, *131*, 110319.
- [38] P. Lv, L. Shi, C. Fan, Y. Gao, A. Yang, X. Wang, S. Ding, M. Rong, *ACS Appl. Mater. Interfaces.* **2020**, *12*, 15012.
- [39] L. Wang, W. Liu, Z. Yan, F. Wang, X. Wang, *Adv. Funct. Mater.* **2021**, *31*, 2007221.
- [40] D. Yang, H. Yang, X. Guo, H. Zhang, C. Jiao, W. Xiao, P. Guo, Q. Wang, D. He, *Adv. Funct. Mater.* **2020**, *30*, 2004514.
- [41] T. G. Weldemhret, J. H. Lee, C. U. Park, D. W. Lee, M. N. Prabhakar, Y. T. Park, J. I. Song, *Sustainable Mater. Technol.* **2024**, *39*, 00847.
- [42] S. Wu, G. Li, W. Liu, D. Yu, G. Li, X. Liu, Z. Song, H. Wang, H. Liu, *Nano Energy* **2022**, *93*, 106859.
- [43] H. Y. Mi, X. Jing, Q. Zheng, L. Fang, H. X. Huang, L. S. Turng, S. Gong, *Nano Energy* **2018**, *48*, 327.
- [44] L. Wang, W. A. Daoud, *Adv. Energy Mater.* **2019**, *9*, 1803183.
- [45] Y. Feng, J. Yu, D. Sun, C. Dang, W. Ren, C. Shao, R. Sun, *Nano Energy* **2022**, *98*, 107284.
- [46] J. Wu, X. Teng, L. Liu, H. Cui, X. Li, *Nano Res.* **2024**, *17*, 5559.

- [47] Y. Wu, J. Qu, X. Zhang, K. AO, Z. Zhou, Z. Zheng, Y. Mu, X. Wu, Y. Luo, S.-P. Feng, *ACS Nano* **2021**, *15*, 13427.
- [48] L.-B. Huang, X. Dai, Z. Sun, M.-C. Wong, S.-Y. Pang, J. Han, Q. Zheng, C.-H. Zhao, J. Kong, J. Hao, *Nano Energy* **2021**, *82*, 105724.
- [49] T. Jing, B. Xu, Y. Yang, M. Li, Y. Gao, *Nano Energy* **2020**, *78*, 105373.
- [50] H. Sun, Y. Zhao, S. Jiao, C. Wang, Y. Jia, K. Dai, G. Zheng, C. Liu, P. Wan, C. Shen, *Adv. Funct. Mater.* **2021**, *31*, 2101696.
- [51] W. Liao, X. Liu, Y. Li, X. Xu, J. Jiang, S. Lu, D. Bao, Z. Wen, X. Sun, *Nano Res.* **2022**, *15*, 2060.
- [52] Q. Zhu, W. Liao, C. Sun, X. Qin, F. Zhang, H. Ji, Y. Li, Z. Wen, X. Sun, *Nano Res* **2023**, *16*, 11638.
- [53] C. Dang, C. Shao, H. Liu, Y. Chen, H. Qi, *Nano Energy* **2021**, *90*, 106619.
- [54] H. Li, F. Xu, T. Guan, Y. Li, J. Sun, *Nano Energy* **2021**, *90*, 106645.
- [55] P. Zhang, Y. Chen, Z. H. Guo, W. Guo, X. Pu, Z. L. Wang, *Adv. Funct. Mater.* **2020**, *30*, 1909252.
- [56] L. Sun, S. Chen, Y. Guo, J. Song, L. Zhang, L. Xiao, Q. Guan, Z. You, *Nano Energy* **2019**, *63*, 103847.
- [57] J. Yang, L. Chang, H. Deng, Z. Cao, *ACS Nano* **2024**, *18*, 18980.
- [58] C. Lu, X. Wang, Y. Shen, C. Wang, J. Wang, Q. Yong, F. Chu, *Adv. Funct. Mater.* **2022**, *32*, 2207714.
- [59] S. Sun, S. Hao, Y. Liu, S. Sun, Y. Xu, M. Jiang, C. Shao, J. Wen, R. Sun, *ACS Nano* **2024**, *19*, 811.
- [60] H. Patnam, S. A. Graham, P. Manchi, M. V. Paranjape, J. S. Yu, *ACS Appl. Mater. Interfaces.* **2023**, *15*, 16768.
- [61] Y. Lin, S. Duan, D. Zhu, Y. Li, B. Wang, J. Wu, *Adv. Intell. Sys.* **2023**, *5*, 2100120.
- [62] A. K. Das, M. Sharma, D. Mondal, K. Prasad, *Carbohydr. Polym.* **2016**, *136*, 930.